Chapter 1

Detection of dark spins via cross-relaxations

In this chapter, we will see how...

1.1 Flip-Flops, double flips and cross-relaxation

The dominant form of interaction between two distant spins is the magnetic dipole-dipole interaction. For two spins with with vector spin Hamiltonian $\hat{\mathbf{S}}_1$ and $\hat{\mathbf{S}}_2$, separated by a distance $\mathbf{r} = r\mathbf{u}$, the dipole-dipole interaction Hamiltonian reads (see Appendix A) :

$$\mathcal{H}_{dd} = \frac{J_0}{r^3}\left[\hat{\mathbf{S}}_1 \cdot \hat{\mathbf{S}}_2 - 3(\hat{\mathbf{S}}_1 \cdot \mathbf{u})(\hat{\mathbf{S}}_2 \cdot \mathbf{u})\right], \tag{1.1}$$

where $J_0 = \frac{\mu_0 \gamma_1 \gamma_2 \hbar^2}{4\pi}$. For two electronic spins with $g-$factors close to 2 (which is the case for the NV center and most spin defect in diamond), the numerical value of J_0 is $(2\pi)\,52$ MHz $\cdot$ nm^3.

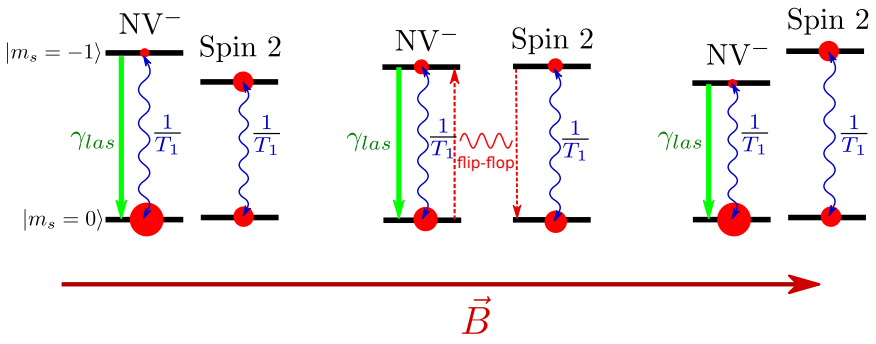

Figure 1.1: Illustration of cross-relaxations between an NV center and an unpolarized spin. Red dots represent the population in each states, and the arrows the various population transfer mechanisms

Flip-flop, in the context of dipole-dipole interaction, is the mechanism which exchanges a quantum of spin between two spins. For an initial state of two spins $\left|m_s^1 = i; m_s^2 = j\right\rangle$, a flip-flop process will result in a final state $|i+1; j-1\rangle$ or $|i-1; j+1\rangle$. The effective rate of this process depends on the matrix element $\langle i; j|\mathcal{H}_{dd}|i \pm 1; j \mp 1\rangle$, as well as the resonance condition between the initial and final state. We should note that for two identical spins, the flip-flop process $|i; i \pm 1\rangle \langle i \pm 1, i|$ is always resonant.

Another mechanism authorized by the dipole-dipole Hamiltonian is the double-flip, either up or down, which couple the states $|i; j\rangle$ and $|i-1; j-1\rangle$ or $|i+1; j+1\rangle$. For a single spin species in a strong magnetic field, the lift of the various spin levels by the Zeeman effect means that no double-flip process can be resonant. However with weak magnetic field or when two different spin species are present, double flip process can be as important as flip-flops since the matrix elements $\langle i; j|\mathcal{H}_{dd}|i \pm 1; j \pm 1\rangle$ are typically of the same order of magnitude as the flip-flop ones.

Cross-relaxation (CR) is the transfer of polarization from one spin to another (or more generally from one family of spins to another family). This process con occur either through flip-flops, or through double flips, as long as the resonance condition between the two spins is met.

Fig. 1.1 illustrates CR between a polarized NV center and an unpolarized second spin. When the two considered spin transitions become resonant, in this case by tuning a magnetic field, polarization from the NV center will be transferred to the second spin, meaning in this case that the NV center will end up less polarized and the second spin more polarized.

The reason why CR tend to depolarize the NV center simply comes from a rate equation : since the initial NV population is higher in the $|0\rangle$ state than in the $|-1\rangle$ state, the flip-flop (or double flip) process that makes the NV center go to $|-1\rangle$ (symbolized by the two red arrows in Fig. 1.1) is more likely than the reverse flip-flop. If we only focus on the NV center, cross-relaxation is simply another thermalization process due to the coupling of the NV center to its environment.

If we make the assumption that the spin bath coupled to the NV centers is Markovian, meaning that the dynamics of the bath is not affected by its coupling to the NV centers, we can then compute the modification in the NV relaxation rate $\Gamma_1 = \frac{1}{T_1}$ due to its coupling to Spin 2 [1]:

$$\delta\Gamma_1 = \frac{\Omega^2}{\Gamma_2^*} \frac{(\Gamma_2^*)^2}{(\delta\nu)^2 + (\Gamma_2^*)^2}, \tag{1.2}$$

where $\Omega = \frac{\langle i;j|\mathcal{H}_{\mathrm{dd}}|j;i\rangle}{\hbar}$ is the matrix element of the dipole-dipole Hamiltonian that couples the initial and final states, $\Gamma_2^* = \frac{1}{T_2^*(\mathrm{NV})} + \frac{1}{T_2^*(\mathrm{Spin2})}$ is the joint dephasing rate of the NV center and the second spin, and $\delta\nu$ is the detuning between the central frequencies of the NV center and spin 2.

1.2 The dark spins in diamond

We refer by dark spins to spin defects which do not interact with light, which in the case of diamond defects consist of every known spin defect bar the NV center and the more recently found ST1 center [2, 3].

1.2.1 P1 centers and ^{13}C

By far the most common spin defects in NV-rich diamond, outside of NV centers, are the substitutional nitrogen centers N_S^0 known as the P1 centers, which have an electronic spin 1/2 and a nuclear spin 1, and the ^{1}3C 1/2 nuclear spin which is present at 1.1% in natural abundance carbon, the remaining carbon atoms being almost exclusively the spinless ^{1}2C isotope.

In NV-rich diamonds, these two impurities are the main causes of the inhomogeneous dephasing rate $\Gamma_2^* = 1/T_2^*$ of the NV centers ensemble [4]. The dephasing comes from the distribution of dipole-dipole coupling from each NV centers to its neighboring spin defects, which varies in space and time.

The dephasing rate caused by a given impurity is directly proportional to the diagonal dipole-dipole matrix elements [5]:

$$\Gamma_2^*(P1) \propto \Omega_{\mathrm{NV-P1}} = \frac{1}{\hbar}\sqrt{\sum_j |\langle NV = i; P1 = j|\mathcal{H}_{\mathrm{dd}}|NV = i; P1 = j\rangle|^2}. \tag{1.3}$$

Since the dipole-dipole coupling rate scales as $1/r^3$, and the distance r between each spin scales as the inverse cubic root of the concentration, it is expected that the dephasing rate associated with a particular impurity scales linearly with the concentration of the impurity. In the case of P1 centers, this was verified experimentally by [5] who found a value of $\Gamma_2^*(\mathrm{P1}) = (2\pi)16$ kHz/ppm.

^{13}C is much more abundant than P1 center ($\sim$ 10 000 ppm at natural abundance) but being a nuclear spin, it has a gyromagnetic ratio $\approx 2.8\,10^3$ times smaller than that of the P1. This results in a contribution to $\Gamma_2^* \sim 10^3$ times smaller per impurity. It was found experimentally that the broadening caused by ^{1}3C is $\Gamma_2^*(^{13}C) \approx 16$ Hz/ppm [6, 4]. For natural abundance diamond, this means that $\Gamma_2^*(^{13}C) \approx 160$ kHz.

1.2.2 Other spin defects, VH^-, War1

Other spin defects are also commonly found in diamond containing NV centers, such as charged vacancy or vacancy clusters [7], other nitrogen related defects [8], transition metals [9], and especially for CVD grown diamond, hydrogen related defects [10], since the CVD plasma contains up to 95 % hydrogen.

Of particular interest in this chapter are two defects: the VH^- defect [11, 12] and the War1 defect [13].

The VH^- defect, prior to our observations, had only been observed *via* electron paramagnetic resonance (EPR) in CVD grown diamond. It is formed by a vacancy with a hydrogen atom bonded to one of the four dangling carbon bond, with an extra electron trapped in the vacancy. This defect has a similar electronic structure to the NV^- which results in an electronic spin-1 with a similar zero field splitting parameter (see Table [REF]). Although the presence of hydrogen in this defect was confirmed by isotopic study, it has been debated whether this defect was VH^- or V_2H^- due to a conflict with *ab initio* calculations [14]. The defect is therefore sometimes referred as V_nH^-. In this manuscript I will employ the original name VH^-.

The War1 defect, named after the University of Warwick where it was first observed in a CVD diamond [13], is another spin-1 defect whose chemical structure remains unknown. No hyperfine structure could be discerned in the relatively broad EPR line, and the use of deuterium instead of ^1H did not change the shape of the line.

1.3 NV center relaxometry

1.3.1 Principle of NV center Relaxometry

Detection *via* cross-relaxation with NV centers fall under the more general technique of NV relaxometry, where we are effectively measuring a modification in the NV center spin lifetime T_1. Relaxometry with NV centers has been used not only to measure resonant cross-relaxation with dark spins [15, 16, 17, 18, 1, 19, 20, 21, 22], but also to probe the magnetic noise in the diamond environment coming from spins [23], ions[24], free radicals [25], magnetic domains [26]...

There can be several advantages to use relaxometry protocols, which measures a change in the NV T_1, over the more common magnetometry protocols that rely on a change in the NV T_2 or T_2^*: the first and most obvious one is that relaxometry does not need to use an external microwave field. This however comes at the cost of a greater precision needed on the external magnetic field. Relaxometry also allows AC-magnetic field sensing in the GHz regime, where traditional microwave-based AC-megnetometry is limited to tens of MHz [27, 28]. Finally, relaxometry measurement can be more sensitive than the T2-based one in some instances [23], which comes from the fact that changes in NV T_1 times are easier to detect than changes in T_2 or T_2^* since T_1 is much longer than T_2 or T_2^*.

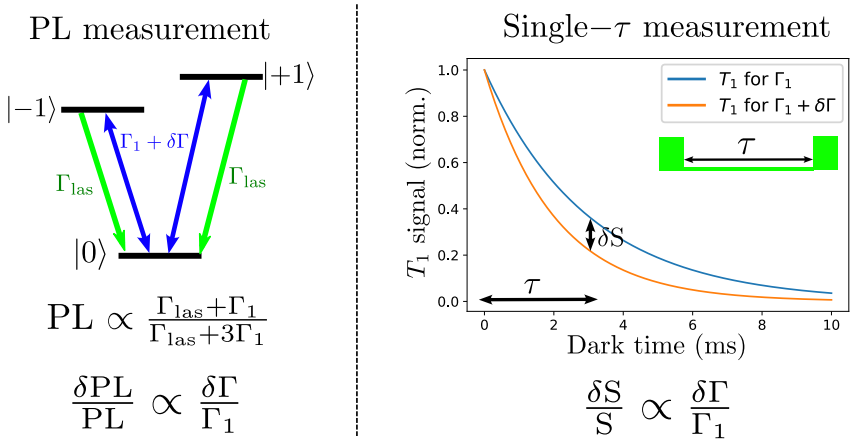

Figure 1.2: Representation of the two relaxometry protocol. Left : representation of the three level system of the NV center with the polarization rate Γ_{las} and spin decay rates $\Gamma_1 = 1/T_1$ and the perturbation $\delta\Gamma$. Right: simulation of a T_1 measurement for $1/\Gamma_1 = 3$ ms and $1/(\Gamma_1 + \delta\Gamma) = 2$ ms. δS represents the maximum difference in signal between the two curves for a dark time τ.

1.3.2 PL and single$-\tau$ relaxometry protocols

There are two ways to measure a change in the spin T_1, as represented on Fig. 1.2. The first and most basic method simply consist in monitoring the PL of the NV centers : since the PL is proportional to the population in the $|0\rangle$ state, which itself results from an equilibrium between the polarization rate Γ_{las} and the spin decay rate $\Gamma_1 = 1/T_1$. A change in Γ_1 will therefore conduct to a new equilibrium with a different PL. For a small enough change $\delta\Gamma << \Gamma_1$, we can consider that we remain in the linear regime, hence why $\frac{\delta PL}{PL} \propto \frac{\delta\Gamma}{\Gamma_1}$.

The second method is a pulsed sequence referred as single$-\tau$ measurement, used for example in [29, 30, 31]. It simply consists in a T_1 measurement sequence (as seen in chapter 1) where you first polarize the spins in the $|0\rangle$ state with a laser pulse and read out the spin state with a second laser pulse after a dark time τ. In this case however, instead of scanning the time τ, you fix its value to maximize the sensitivity in a change of T_1 (typically $\tau \approx T_1$). Again, assuming you are in the linear regime, you observe a change in signal proportional to the change in Γ_1 : $\frac{\delta S}{S} \propto \frac{\delta\Gamma}{\Gamma_1}$.

It is argued in [26] that both methods result in similar signal to noise ratio: in the first case you need to adjust $\Gamma_{las} \sim \Gamma_1$ to maximize the PL contrast, meaning that the laser power used is very far from the saturation limit (typically $\Gamma_1 \approx 10^3$ s^{-1} and $\Gamma_{sat} = 5 \cdot 10^6$ s^{-1}[32]), while the second method needs to wait a time $\tau \sim T_1$ between each measurement, which result in a similar PL count and shot noise limit in both case.

On a technical level, the PL-based method is easier to implement since it does not require the use of a pulsed laser, and uses an overall smaller laser power, however it is more sensitive to drifts and changes in the optical setup. Most of the relaxometry measurement in this manuscript were performed using a PL-based detection.

1.3.3 Comparison with DEER protocol

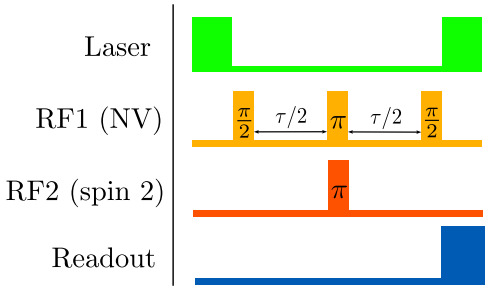

Figure 1.3: Pulse sequence of the DEER protocol

Outside of cross-relaxations, another protocol exists to address dark spin resonance with NV centers, based on a modification of the NV T_2 time [33]. This protocol called double electron-electron resonance (DEER) is depicted on Fig. 1.3. The pulse sequence consist in a spin-echo sequence on the NV center, as described in chapter 1, with a simultaneous $\pi-$pulse on the probed dark spins during the rephasing pulse on the NV centers. This additional pulse means that the static (or slowly variable) contribution of the probed spins to the T_2^* of the NV center wont be rephased. The newly measured T_2 time should therefore be slightly shorter:

$$\frac{1}{T_2^{\text{DEER}}} = \frac{1}{T_2^{\text{echo}}} + \delta\Gamma, \tag{1.4}$$

where $\delta\Gamma$ is the contribution of the dark spin to the T_2^* of the NV center through NV-dark spin dipole-dipole interaction.

By scanning the frequency of the second microwave (RF2) and monitoring the T_2 time of the NV centers, one can therefore find dark spin resonance without having to bring them to resonance with NV centers, which can be useful when the dark spin resonance is very far detuned from the NV one.

While both cross-relaxation and DEER measure the dipole-dipole coupling of dark spins to an NV center, there are several differences between the two protocols:

Frist, the two protocols do not measure the same elements of the dipole-dipole Hamiltonian: CR measures the off-diagonal elements $\Omega_{\text{CR}} = \langle i,j|\mathcal{H}_{\text{dd}}|j,i\rangle/\hbar$ which are responsible for the flip-flops or double flips, while DEER measures the diagonal elements $\Omega_{\text{DEER}} = \langle i,j|\mathcal{H}_{\text{dd}}|i,j\rangle/\hbar$ which are responsible for

the pure dephasing. These terms however are on average of the same amplitude, and when averaging over an ensemble we can consider $\Omega_{CR} \sim \Omega_{DEER}$

Second and more importantly, the scaling is not the same in both cases : CR measures a change in the NV decay rate $\Gamma_1 = 1/T_1$ which is proportional to Ω_{CR}^2, as given by eq. 1.2, while DEER measures a change in $\Gamma_2 = 1/T_2$ which is proportional to Ω_{DEER}, as given by eq. 1.3. This means that the signal of CR scales quadratically with the impurity concentration, while the DEER signal scales linearly with it. CR is therefore more suited to probe concentrated impurities, when the average distance between the NV and the probed spin is small.

1.4 Choice of the magnetic field orientation

Since relaxometry does not rely on a microwave field, the only parameter left to tune is the external magnetic field, which is often scanned with an electromagnet. Due to the strong NV anisotropy however, the direction along which **B** is scanned plays a crucial role in the ability to detect dark spins.

1.4.1 The [100] and [111] magnetic field orientations

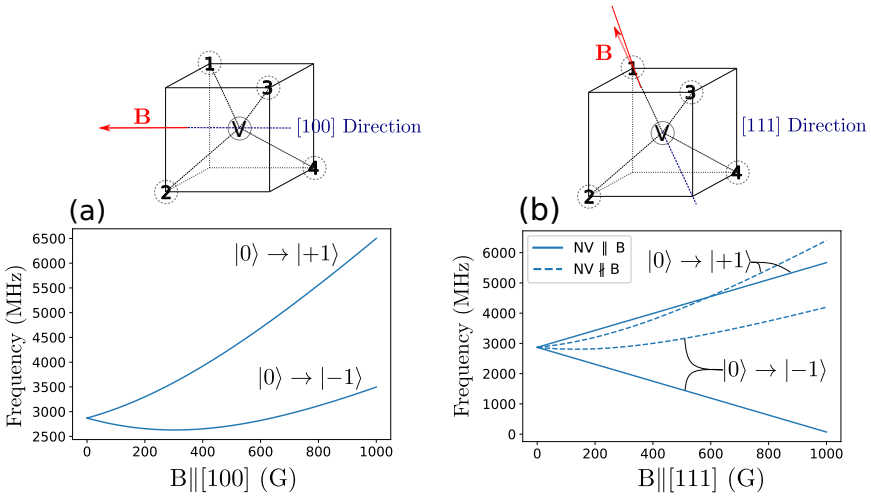

Figure 1.4: Label

Fig. 1.4 shows the two main choices of scanning orientation : either **B** ∥ [100] or **B** ∥ [111] where [100] and [111] refer to the diamond crystalline axes as defined in chapter 1. When **B** ∥ [100], all four classes (the different possible NV orientations represented at the top of the figure) are equivalent, whereas for **B** ∥ [111], one class is perfectly aligned with the magnetic field while the three others are equivalently unaligned.

These changes in the field orientation result in massive changes in the NV behavior, manly due to the transverse magnetic field: Fig. 1.4-a) shows the transition frequency between the $|0\rangle$ and $|\pm 1\rangle$ states of the ground state spin Hamiltonian (REF chapter 1) - or to be more precise the transitions between the ground state of the spin Hamiltonian and the two excited states - for any of the four classes of NV centers when $\mathbf{B} \parallel [100]$. Notably, there is no transitions frequencies below 2500 MHz.

On the other hand, Fig. 1.4-b) shows the transition frequencies when $\mathbf{B} \parallel [111]$, for both the class aligned and the three class misaligned. The three classes behave similarly than the four classes in the [100] case, but the one class aligned with the magnetic field can get its $|0\rangle \rightarrow |-1\rangle$ transition arbitrarily small, as long as the magnetic field is perfectly aligned with the NV axis.

1.4.2 CR condition between NV^- and P1

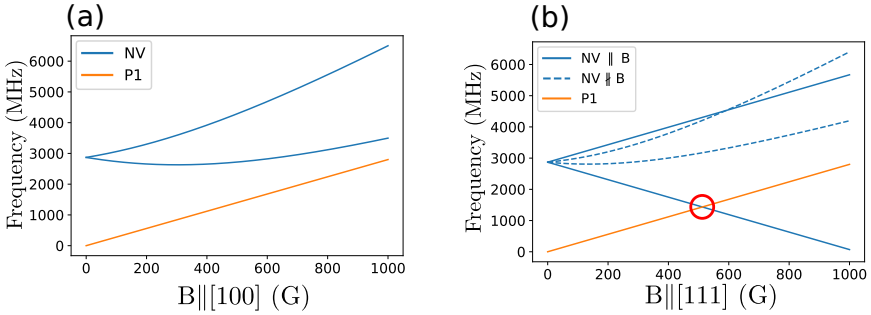

Figure 1.5: Label

P1 centers, the most abundant electronic spin in the diamonds commonly used, have a 1/2 electronic spin. They do have a small magnetic field anisotropy coming from the hyper-fine coupling to the nitrogen nucleus ($\sim$ 100 MHz), but this dependency on the field orientation is small compared to the NV center's zero field splitting $D = 2870$ MHz. We can therefore, to the first order, neglect the hyper-fine coupling and consider P1 centers as ideal, isotropic, spin 1/2.

Fig. 1.5 shows the transition frequencies for the NV center and such a spin 1/2, as a function of a magnetic field parallel to [100] or [111]. When $\mathbf{B} \parallel [100]$, there will never be a co-resonance between the NV and P1 transitions, meaning that no NV-P1 cross-relaxation can be observed when B is scanned in this direction. When $\mathbf{B} \parallel [111]$ however, the P1 $|-1/2\rangle \rightarrow |+1/2\rangle$ transition matches in energy the $|0\rangle \rightarrow |-1\rangle$ NV transition for B=512 G. This means that when B reaches $\approx$ 512 G, some of the polarization of the NV centers will be transferred to the P1 centers, which will result in a drop in the NV PL.

1.4.3 CR condition between NV^- and VH^-

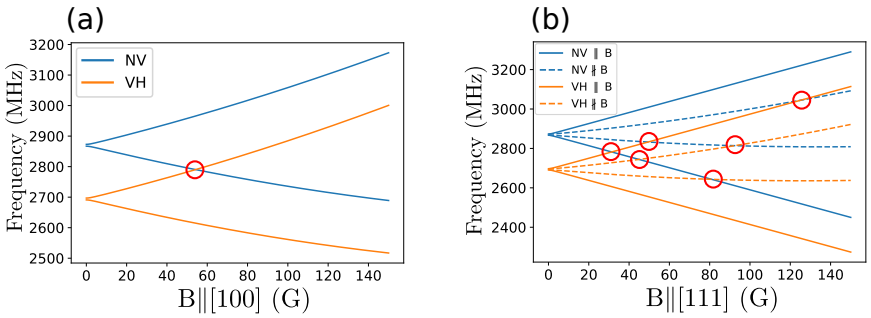

Figure 1.6: Label

VH^-, a much less abundant electronic spin than P1 center, has an electronic spin 1, with a spin Hamiltoninan very similar to that of the NV center. In particular it has the same symmetries being also a C_{3v} defect, with a slightly smaller ZFS at $D_{VH} \approx 2700$ MHz compared to $D_{NV} = 2870$ MHz.

Fig. 1.6 shows the transition frequencies for the NV^- and VH^- ground state spin. Contrary to the P1 case, there is a co-resonance when $\mathbf{B} \parallel [100]$ for $B \approx 55$ G. When $\mathbf{B} \parallel [111]$, there are 6 co-resonance conditions between 30 and 130 G. A scan along the [111] in this case means that the peak signal is ~ 6 times weaker than in the [100] case, and spread over multiple features which might overlap between themselves or with other existing PL features.

The War1 spin mentioned previously is also an electronic spin 1 with (pseudo)-C_{3v} symmetry and $D_{War1} \approx 2470$ MHz. This result in a similar behavior than VH^- when it comes to the CR condition with NV centers.

1.4.4 CR condition between NV^- and and ^{13}C-NV^-

I refer by ^{13}C-NV^- to a complex formed by an NV center where one of the three carbon atoms neighboring the vacancy is a ^{13}C isotope, which is illustrated in Fig. 1.7-a).

The ^{13}C-NV^- complex still behaves as a "normal" NV center, except with shifted transition lines. In particular its electronic spin is still polarized in the $|0\rangle$ state and the $|0\rangle$ state is still brighter than the $|\pm 1\rangle$ states. This is confirmed by the presence of sideband in ODMR spectra around the main NV lines [34].

Since both NV^- and ^{13}C-NV^- are *a priori* equally polarized, then following the argument in 1.1 there should be no CR between the two spin families. The reason why those transitions are still in some case visible, as will be shown below, and why in fact any NV-NV co-resonance gives a visible CR signal will be the object of the next chapter.

The transitions of the ^{13}C-NV^- complex are given by diagonalizing the

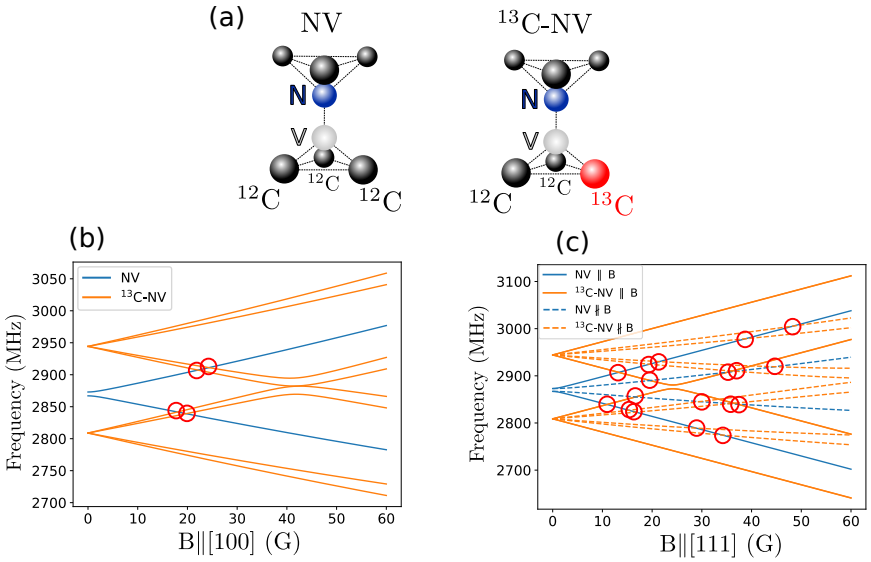

Figure 1.7: Label

full spin Hamiltonian:

$$\mathcal{H} = \mathcal{H}_{NV} + \mathcal{H}_{^{13}C} + \mathcal{H}_{HF},$$

where $\mathcal{H}_{NV}$ is the NV$^-$ spin Hamiltonian, $\mathcal{H}_{^{13}C}$ is the ^{13}C nuclear spin Hamiltonian for a 1/2 spin : $\mathcal{H}_{^{13}C} = \gamma_n B I_z$ where γ_n =10.7 MHz/T is the ^{13}C gyromagnetic ratio, and $\mathcal{H}_{HF}$ is the hyper-fine interaction Hamiltonian:

$$\mathcal{H}_{HF} = \hat{\mathbf{S}}_{NV} \cdot \mathcal{A} \cdot \hat{\mathbf{I}}_C.$$

When the ^{13}C is the direct neighbor of the vacancy as represented in Fig. 1.7-a) - this is also referred as a first-shell ^{13}C - the hyper-fine tensor $\mathcal{A}$ can be written [34]:

$$\mathcal{A} = \begin{pmatrix} \mathcal{A}_{xx} & 0 & \mathcal{A}_{xz} \\ 0 & \mathcal{A}_{yy} & 0 \\ \mathcal{A}_{zx} & 0 & \mathcal{A}_{zz} \end{pmatrix},$$

where $\mathcal{A}_{xx} = 190$ MHz, $\mathcal{A}_{yy} = 120$ MHz, $\mathcal{A}_{zz} = 129$ MHz, and $\mathcal{A}_{xz} = \mathcal{A}_{zx} = -25.0$ MHz.

Fig. 1.7-b) and c) show the simulated transition frequencies for a ^{13}C-NV$^-$ complex when B is scanned along the [100] or [111] axis, as well as the "normal" NV transitions and the co-resonance between those two. When $\mathbf{B} \parallel [100]$, there are 4 co-resonances between 18 and 25 G. When $\mathbf{B} \parallel [100]$ there are 18 of them between 10 and 60 G. This abundance of transitions for low (¡100 G) magnetic field makes analyzing experimental data quickly intractable in the second case.

1.4.5 CR contrast and transverse magnetic field

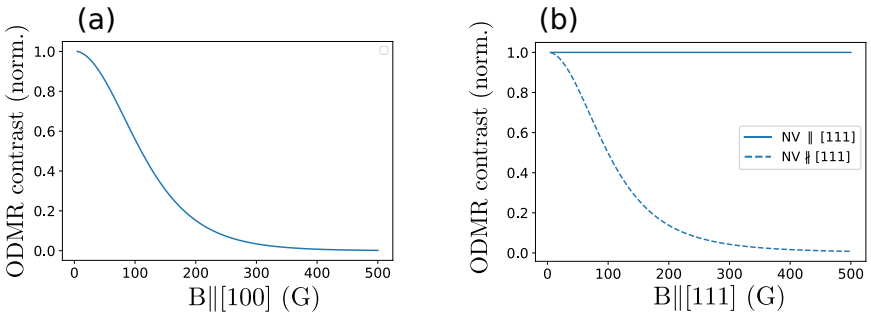

Figure 1.8: Label

In order to optically detect CR between an NV center and a dark spin, two conditions must be met: the NV center must be polarized in order to have a population transfer between the NV and the dark spin, and there must be a difference in brightness between the two NV levels involved in order to have an optical signature of the CR.

These two conditions are in fact the same needed to observe an ODMR spectrum (REF chapter 1), and while the NV centers verifies both criteria in presence of a purely longitudinal magnetic field, this is not always the case anymore in presence of a transverse magnetic field (REF chapter 1).

Fig. 1.8 shows the simulated relative contrast of an ODMR spectrum, as computed from [35], for a magnetic field aligned along [100] or [111]. When the NV center is aligned with the magnetic field, the constrats remains equals to 1 regardless of the magnetic field because there is no transverse field. When the NV is not aligned however, either in the [111] or [100] case, the ODMR contrast quickly drops down for B$>$ 100 G.

This tells us that we should not expect to observe a CR signal for B greater than a few hundreds G when B is scanned along the [100] axis. We could however observe CR for arbitrarily large magnetic field when scanned along the [111] axis, as long as the field is properly aligned with the NV axis.

1.5 Dark spin spectroscopy with NV centers

1.5.1 Detection of P1 centers

Previously to our work, several studies [15, 16, 17, 18, 1, 19, 20, 21, 22] had been done on the detection of dark spins through CR with NV centers, and to our knowledge, all this studies where done on the detection of P1 centers. Following the discussion in the last section, these studies were therefore all done with $\mathbf{B} \parallel [111]$.

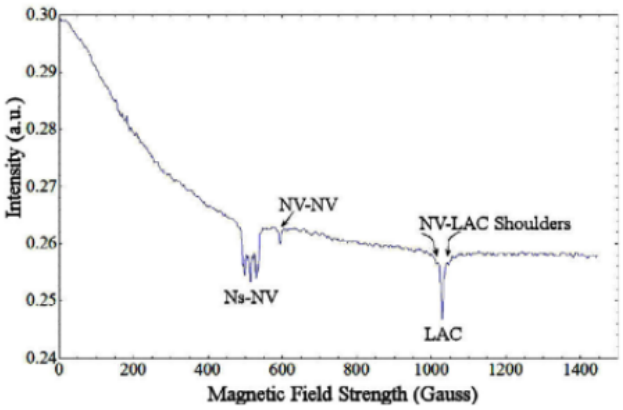

Figure 1.9: Taken from [18]Label

An example of one of this study ([18]) is shown in Fig. 1.9. It shows the evolution of the NV PL with respect to a magnetic field scanned along the [111] crystalline axis. There are several information to gather from this graph:

First, there is the slowly decaying PL envelope, which stabilizes to a plateau for $B \sim 1000$ G. This change in PL is caused by the transverse magnetic field acting on the three NV classes that are not aligned with the magnetic field. For $B \gtrsim 1000$ G, these three classes are fully depolarized which explains the plateau observed.

Second, there are the three salient features denoted Ns-NV, NV-NV and NV-LAC. All these features come from cross-relaxations or level anti-crossing (LAC) from the NV class aligned with the magnetic field.

The first feature (Ns-NV) for $B \approx 512$ G is the signature of the CR between NV and P1 centers. Its relatively complicated shape comes from the hyper-fine coupling between the P1 electronic spin and the ^{1}4N nucleus [22]. Excited state level anti-crossing (ESLAC) also occurs in this region, but its optical signature, if it exists, is expected to be much weaker than the NV-P1 CR [36].

The second feature (NV-NV) for $B \approx 590$ G comes from the cross relaxation between NV centers aligned with the magnetic field and NV centers misaligned with the field (the co-resonance can be observed in Fig. 1.4-b)). This phenomenon will be further discussed in the next chapter.

Finally the third feature (LAC) for $B \approx 1024$ G correspond to the level anti-crossing between the $|0\rangle$ and $|-1\rangle$ states of the NV center aligned with B. When the two levels get close enough in energy, the Hamiltonian off-diagonal terms (coming from strain local electric field or residual transverse magnetic field) will mix the $|0\rangle$ and $|-1\rangle$ states and prevent an efficient polarization by the green laser. This result in a sharp drop in the PL that can be exploited to perform microwave-less magnetometry with NV centers

[19, 36, 37].

1.5.2 Detection of VH^- and War1 defects

During my PhD, I have studied the Our work [38]

1.6 Attribution of the VH^- and War1 lines

Bibliography

[1] LT Hall et al. "Detection of nanoscale electron spin resonance spectra demonstrated using nitrogen-vacancy centre probes in diamond". In: *Nature communications* 7.1 (2016), pp. 1–9.

[2] Sang-Yun Lee et al. "Readout and control of a single nuclear spin with a metastable electron spin ancilla". In: *Nature nanotechnology* 8.7 (2013), pp. 487–492.

[3] Roger John et al. "Bright optical centre in diamond with narrow, highly polarised and nearly phonon-free fluorescence at room temperature". In: *New Journal of Physics* 19.5 (2017), p. 053008.

[4] John F Barry et al. "Sensitivity optimization for NV-diamond magnetometry". In: *Reviews of Modern Physics* 92.1 (2020), p. 015004.

[5] Erik Bauch et al. "Decoherence of ensembles of nitrogen-vacancy centers in diamond". In: *Physical Review B* 102.13 (2020), p. 134210.

[6] JA Van Wyk et al. "The dependences of ESR line widths and spin-spin relaxation times of single nitrogen defects on the concentration of nitrogen defects in diamond". In: *Journal of Physics D: Applied Physics* 30.12 (1997), p. 1790.

[7] LS Hounsome et al. "Origin of brown coloration in diamond". In: *Physical Review B* 73.12 (2006), p. 125203.

[8] ME Newton. "EPR, ENDOR and EPR Imaging of Defects in Diamond". In: *Electron Paramagnetic Resonance* 20 (2007), pp. 131–156.

[9] J Isoya et al. "Fourier-transform and continuous-wave EPR studies of nickel in synthetic diamond: Site and spin multiplicity". In: *Physical Review B* 41.7 (1990), p. 3905.

[10] Christopher Brett Hartland. "A study of point defects in CVD diamond using electron paramagnetic resonance and optical spectroscopy". PhD thesis. University of Warwick UK, 2014.

[11] Claire Glover et al. "Hydrogen incorporation in diamond: The nitrogen-vacancy-hydrogen complex". In: *Physical review letters* 90.18 (2003), p. 185507.

[12] Claire Glover et al. “Hydrogen incorporation in diamond: The vacancy-hydrogen complex”. In: *Physical review letters* 92.13 (2004), p. 135502.

[13] Robin Cruddace. “Magnetic resonance and optical studies of point defects in single crystal CVD diamond”. PhD thesis. University of Warwick, 2007.

[14] MJ Shaw et al. “Importance of quantum tunneling in vacancy-hydrogen complexes in diamond”. In: *Physical review letters* 95.10 (2005), p. 105502.

[15] Eric van Oort and Max Glasbeek. “Cross-relaxation dynamics of optically excited N-V centers in diamond”. In: *Physical Review B* 40.10 (1989), p. 6509.

[16] K Holliday et al. “Optical hole-bleaching by level anti-crossing and cross relaxation in the NV centre in diamond”. In: *Journal of Physics: Condensed Matter* 1.39 (1989), p. 7093.

[17] RJ Epstein et al. “Anisotropic interactions of a single spin and dark-spin spectroscopy in diamond”. In: *Nature physics* 1.2 (2005), pp. 94–98.

[18] Seiji Armstrong et al. “NV–NV electron–electron spin and NV–NS electron—electron and electron-nuclear spin interaction in diamond”. In: *Physics Procedia* 3.4 (2010), pp. 1569–1575.

[19] Arne Wickenbrock et al. “Microwave-free magnetometry with nitrogen-vacancy centers in diamond”. In: *Applied Physics Letters* 109.5 (2016), p. 053505.

[20] James DA Wood et al. “Wide-band nanoscale magnetic resonance spectroscopy using quantum relaxation of a single spin in diamond”. In: *Physical Review B* 94.15 (2016), p. 155402.

[21] Nir Alfasi et al. “Detection of paramagnetic defects in diamond using off-resonance excitation of NV centers”. In: *Physical Review B* 99.21 (2019), p. 214111.

[22] Reinis Lazda et al. “Cross-relaxation studies with optically detected magnetic resonances in nitrogen-vacancy centers in diamond in external magnetic field”. In: *Physical Review B* 103.13 (2021), p. 134104.

[23] S Steinert et al. “Magnetic spin imaging under ambient conditions with sub-cellular resolution”. In: *Nature communications* 4.1 (2013), pp. 1–6.

[24] J-P Tetienne et al. “Spin relaxometry of single nitrogen-vacancy defects in diamond nanocrystals for magnetic noise sensing”. In: *Physical Review B* 87.23 (2013), p. 235436.

[25] Linyan Nie et al. “Quantum sensing of free radicals in primary human dendritic cells”. In: *Nano letters* 22.4 (2021), pp. 1818–1825.

[26] Aurore Finco et al. “Imaging non-collinear antiferromagnetic textures via single spin relaxometry”. In: *Nature communications* 12.1 (2021), pp. 1–6.

[27] Zhecheng Wang et al. “Picotesla magnetometry of microwave fields with diamond sensors”. In: *arXiv preprint arXiv:2206.08533* (2022).

[28] Scott T Alsid et al. “A Solid-State Microwave Magnetometer with Picotesla-Level Sensitivity”. In: *arXiv preprint arXiv:2206.15440* (2022).

[29] Matthew Pelliccione et al. “Two-dimensional nanoscale imaging of gadolinium spins via scanning probe relaxometry with a single spin in diamond”. In: *Physical Review Applied* 2.5 (2014), p. 054014.

[30] Dominik Schmid-Lorch et al. “Relaxometry and dephasing imaging of superparamagnetic magnetite nanoparticles using a single qubit”. In: *Nano letters* 15.8 (2015), pp. 4942–4947.

[31] Jean-Philippe Tetienne et al. “Scanning nanospin ensemble microscope for nanoscale magnetic and thermal imaging”. In: *Nano Letters* 16.1 (2016), pp. 326–333.

[32] A Dréau et al. “Avoiding power broadening in optically detected magnetic resonance of single NV defects for enhanced dc magnetic field sensitivity”. In: *Physical Review B* 84.19 (2011), p. 195204.

[33] Maksym Serbyn et al. “Interferometric probes of many-body localization”. In: *Physical review letters* 113.14 (2014), p. 147204.

[34] Maria Simanovskaia et al. “Sidebands in optically detected magnetic resonance signals of nitrogen vacancy centers in diamond”. In: *Physical Review B* 87.22 (2013), p. 224106.

[35] JP Tetienne et al. “Magnetic-field-dependent photodynamics of single NV defects in diamond: an application to qualitative all-optical magnetic imaging”. In: *New Journal of Physics* 14.10 (2012), p. 103033.

[36] Huijie Zheng et al. “Level anti-crossing magnetometry with color centers in diamond”. In: *Slow Light, Fast Light, and Opto-Atomic Precision Metrology X*. Vol. 10119. SPIE. 2017, pp. 115–122.

[37] Huijie Zheng et al. “Microwave-free vector magnetometry with nitrogen-vacancy centers along a single axis in diamond”. In: *Physical Review Applied* 13.4 (2020), p. 044023.

[38] Clément Pellet-Mary et al. “Optical detection of paramagnetic defects in diamond grown by chemical vapor deposition”. In: *Physical Review B* 103.10 (2021), p. L100411.